nature physics

LETTERS

PUBLISHED ONLINE: 16 NOVEMBER 2008 | DOI: 10.1038/NPHYS1133

Tomography of quantum detectors

J. S. Lundeen[1]*, A. Feito[2,3], H. Coldenstrodt-Ronge[1], K. L. Pregnell[2,3], Ch. Silberhorn[4], T. C. Ralph[5], J. Eisert[2,3], M. B. Plenio[2,3] and I. A. Walmsley[1]*

Measurement connects the world of quantum phenomena to the world of classical events. It has both a passive role—in observing quantum systems—and an active one, in preparing quantum states and controlling them. In view of the central status of measurement in quantum mechanics, it is surprising that there is no general recipe for designing a detector that measures a given observable[1]. Compounding this, the characterization of existing detectors is typically based on partial calibrations or elaborate models. Thus, experimental specification (that is, tomography) of a detector is of fundamental and practical importance. Here, we present the realization of quantum detector tomography[2–4]. We identify the positive-operator-valued measure describing the detector, with no ancillary assumptions. This result completes the triad, state[5–11], process[12–17] and detector tomography, required to fully specify an experiment. We characterize an avalanche photodiode and a photon-number-resolving detector capable of detecting up to eight photons[18]. This creates a new set of tools for accurately detecting and preparing non-classical light.

The reduction of the quantum state of a system by measurement, as postulated by von Neumann, is now generally accepted to be a limiting case of a more general theory of quantum measurement that involves state reduction on an extended Hilbert space encompassing the system and an (possibly fictional) ancilla. However, even within this general theory, it is not known how to incorporate the complete chain of apparatus components in a derivation of the actual measurement: as Braginsky has written, "the Schrödinger equation cannot tell us the connection between the design of the measuring device and the nature of the measurement"[1]. Measurement is increasingly becoming a driving component in quantum technologies such as super-resolution metrology[19], Heisenberg-limited sensitivity[20] and quantum computing[21]. Input states and dynamical processes are accepted as resources for quantum technologies and therefore the techniques of quantum state tomography[5–11,22] and quantum process tomography[12–17,23] have been developed to measure them. A distinct omission is that of the experimental tomography of detectors, which would enable more accurate classification of measurement types, objective comparison of competing devices and precise design of new detectors. This omission is even more striking given that the tomography of states and processes are predicated on a well-characterized detector. Here, we extend previous theoretical descriptions of detector tomography[2–4] to include regularization and to accommodate the classical uncertainties of the experimental apparatus. We apply this theory to the characterization of two quantum detectors.

Characterizing a detector consists of determining its corresponding positive-operator-valued measure (POVM). Given an input state ρ, the probability $p_{n,\rho}$ of obtaining detection outcome n is

$$p_{n,\rho} = \mathrm{tr}[\rho\pi_n], \tag{1}$$

where $\{\pi_n\}$ is the detector POVM. In state tomography, an unknown ρ is characterized by carrying out a set of known measurements, each on many identical copies of the state to estimate p_n. From this estimate, one can invert equation (1) to find ρ. The interchangeability of ρ and π_n in equation (1) shows that detector tomography has a dual role to state tomography. Now, measuring a set of known probe states $\{\rho\}$ enables us to characterize an unknown detector, and thus find $\{\pi_n\}$. For these operators to describe a physical measurement apparatus, they must be positive semi-definite, $\pi_n \geq 0$, and $\sum_n \pi_n = I$, ensuring positive probabilities that add up to one. In addition, the operators $\{\rho\}$ must be chosen to be tomographically complete, that is, form a basis for the operator space of π_n.

In the specific case of optical detectors, lasers provide us with an ideal tomographic probe: the coherent state $|\alpha\rangle$. By transforming the magnitude $|\alpha|$ through attenuation (for example, with a beam splitter) and the phase $\arg(\alpha)$ by optical delay, we can create a tomographically complete set of probe states $\{|\alpha\rangle\langle\alpha|\}$. Remarkably, with coherent state probes, the measured statistics are themselves a full representation of the detector. The measurement outcomes sample the function

$$Q_n(\alpha) = \frac{1}{\pi}\langle\alpha|\pi_n|\alpha\rangle = \frac{1}{\pi}p_{n,\alpha}. \tag{2}$$

This is, in fact, a definition of the well-known Q-function representation of the POVM element[2]. As $Q_n(\alpha)$ contains the same information as the element π_n itself, estimation of this function constitutes detector tomography. Predictions of the detection probabilities for arbitrary input states can then be calculated directly from the Q-function representation. Unfortunately, experimental errors and statistical fluctuations can cause a simple fit to the Q-function to be consistent with unphysical POVM elements. Owing to this, we ultimately wish to directly find the POVM elements $\{\pi_n\}$ that are closest to the measured statistics, while constraining them to be physical.

We now turn to the description of the experimental realization, shown in Fig. 1 (see the Methods section). The first detector was a commercial single-photon counting module based on a silicon avalanche photodiode (APD). It has two detection outcomes, either outputting an electronic pulse (1 click) or not (0 clicks). Past evaluation of the detector has shown that the 1-click outcome is mainly associated with the arrival of one or more photons, although dark counts and afterpulsing can also create this outcome. The 0-click event is mainly associated with vacuum at the input

[1]Clarendon Laboratory, Oxford University, Parks Road, Oxford, OX1 3PU, UK, [2]Institute for Mathematical Sciences, Imperial College London, SW7 2PG, UK, [3]QOLS, The Blackett Laboratory, Imperial College London, Prince Consort Road, SW7 2BW, UK, [4]Max-Planck Research Group for Optics, Information and Photonics, 91058 Erlangen, Germany, [5]Department of Physics, University of Queensland, Brisbane, QLD 4072, Australia.
*e-mail: j.lundeen1@physics.ox.ac.uk; walmsley@physics.ox.ac.uk.

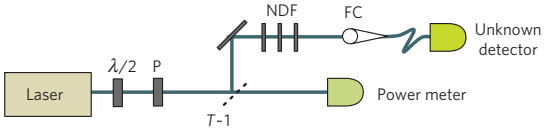

Figure 1 | The experimental set-up. A half-wave plate (λ/2) and Glan–Thompson polarizer (P) are used to vary the amplitude of the probe coherent state, which is subsequently attenuated by neutral density filters (NDF) and coupled into a fibre (FC). See the Methods section for more details.

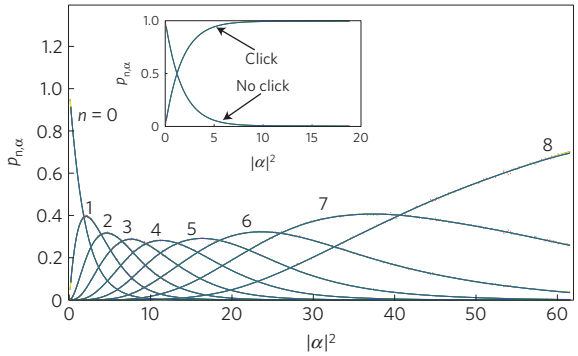

Figure 2 | The detector tomography data. The outcome statistics (red dots) are measured as a function of the coherent state magnitude $|\alpha|^2$ and form an estimate of $p_{n,\alpha}$ for each detector outcome n (number of clicks). As they are proportional to the Q-function $Q_n(\alpha)$ for each outcome, the statistics directly fully characterize the detector. The main plot corresponds to the TMD with nine outcomes and the inset corresponds to the APD. The vertical statistical error is too small to be seen. From the reconstructed POVM elements $\{\pi_n\}$, we generate the corresponding probabilities $p_{n,\alpha} = \langle\alpha|\pi_n|\alpha\rangle$ (blue curves).

or photons lost owing to non-unit efficiency of the photodiode. Having only two outcomes, this detector cannot directly measure the incoming photon number if it is above one. The second detector circumvents this by splitting the incoming pulse into many spatially or temporally separate bins, making unlikely the presence of more than one photon per bin. Subsequently all of the bins are detected with two APDs. Photon-number resolution results by summing the number of 1-click outcomes from all of the bins. This time-multiplexed detector (TMD) is not commercially available but can be constructed with standard tools[18]. Ours has eight bins in total (four time bins in each of two output fibres) and thus nine outcomes—from zero to eight clicks, making it capable of detecting up to eight photons. The added complexity and greater number of outcomes of this detector provide a more challenging test for detector tomography.

For both detectors, we first allowed the phase of α to drift. We observed no variation in the outcome frequencies, as expected from a detector without a phase reference. This simplifies the experimental procedure, requiring us to control only the magnitude of α (as has been done for tomography of a single photon[24]). A detector with no observed phase dependence will be described by POVM elements diagonal in the number basis,

$$\pi_n = \sum_{k=0}^{\infty} \theta_k^{(n)} |k\rangle\langle k|, \tag{3}$$

simplifying henceforth the reconstruction of π_n.

For a POVM set $\{\pi_n\}$ containing only diagonal matrices as in equation (3) that are each truncated at a number state M, we can rewrite equation (2) as a matrix equation,

$$P = F\Pi.$$

For an N-outcome detector, $P_{D\times N}$ contains all of the measured statistics, $F_{D\times M}$ contains the D probe states $\alpha, \alpha_1, \ldots, \alpha_D$ and $\Pi_{M\times N}$ contains the unknown POVM set (matrix subscripts are the matrix dimensions). For a coherent state probe, $F_{i,k} = (|\alpha_i|^{2k}\exp(-|\alpha_i|^2)/k!)$. This can easily be reformulated for a probe in a mixed state, as was done to model the laser technical noise (see the Methods section). The physical POVM consistent with the data can be estimated through the following optimization problem:

$$\min\left\{||P - F\Pi||_2 + g(\Pi)\right\},$$

$$\text{subject to } \pi_n \geq 0, \qquad \sum_{n=0}^{N-1} \pi_n = I, \tag{4}$$

where the 2-norm of a matrix A is defined as $||A||_2 = (\sum_{i,j}|A_{i,j}|^2)^{1/2}$. We regularize the inversion by means of an extra constraint: the specification of a convex quadratic function g, independent of the type of detector, that smooths fluctuations with respect to photon number from element to element of the POVM. This is a convex quadratic optimization problem, and hence also a semi-definite problem[25] which can be efficiently solved numerically. Moreover, in this case, there exists a dual optimization problem in which the solution coincides with the original problem. Thus, the dual problem provides a certificate of optimality that we use to verify our solution. This procedure identifies the optimal POVM for this cost function.

The measured statistics for each detector outcome (that is, the number of clicks) are shown in Fig. 2 for the TMD and for the APD. The distributions (equivalent to the Q-function $Q_n(\alpha)$ of the detector) show smooth profiles and distinct photon number ranges of sensitivity for increasing number of clicks in the detector. Figure 3 shows the diagonals (the off-diagonals are zero for these phase-insensitive detectors) of the POVMs that result from optimization of equation (4) (see the Methods section for $g(\Pi)$). Note that π_n, being the POVM element for n clicks, shows nearly zero amplitude for detecting less than n photons, exhibiting essentially no dark counts. Prominent in an otherwise smooth distribution, this sharp feature provides the detector with its discriminatory power: n clicks guarantees that there were at least n photons in the input pulse. To assess the performance of the tomography, we find the difference (yellow bars in Fig. 3) between the estimated POVM elements π_n^{rec} and a previously developed simple theoretical model of a TMD, π_n^{teo} (ref. 26; see the Methods section). The fidelity $F = \mathrm{tr}((\sqrt{\pi_n^{\mathrm{teo}}}\pi_n^{\mathrm{rec}}\sqrt{\pi_n^{\mathrm{teo}}})^{1/2})^2 \geq 98.7\%$ for all n, indicating excellent agreement between the two.

To visualize the action of the detector, in the special case of optical detectors one can plot a Wigner function of each of the reconstructed POVM elements, $W_n(\alpha, \alpha^*)$. The response of the detector to an input state with Wigner function W_ψ is proportional to the overlap, $p_{n,\psi} = \int W_n W_\psi \, d\alpha d\alpha^*$. We focus on the one-click Wigner function $W_1(\alpha, \alpha^*)$ for the APD (Fig. 4a) and the TMD (Fig. 4b). An APD detector is sometimes regarded as a 'single photon detector', but here we can see the marked difference between the two Wigner functions. Instead, it is the TMD that has a fidelity of 98% with a single photon (having experienced a 52.2% loss). Conversely, the APD Wigner function extends to $\alpha \gg 1$, having significant overlap with photon number states $\geqslant 1$. Therefore, to use an APD as a 'single-photon detector' one must make the ancillary assumption that the input beam has insignificant components containing more than one photon. Despite their differences, both Wigner functions have negative values near the origin, indicating the absence of a classical optical analogue. Consequently, these are both fundamentally quantum detectors.

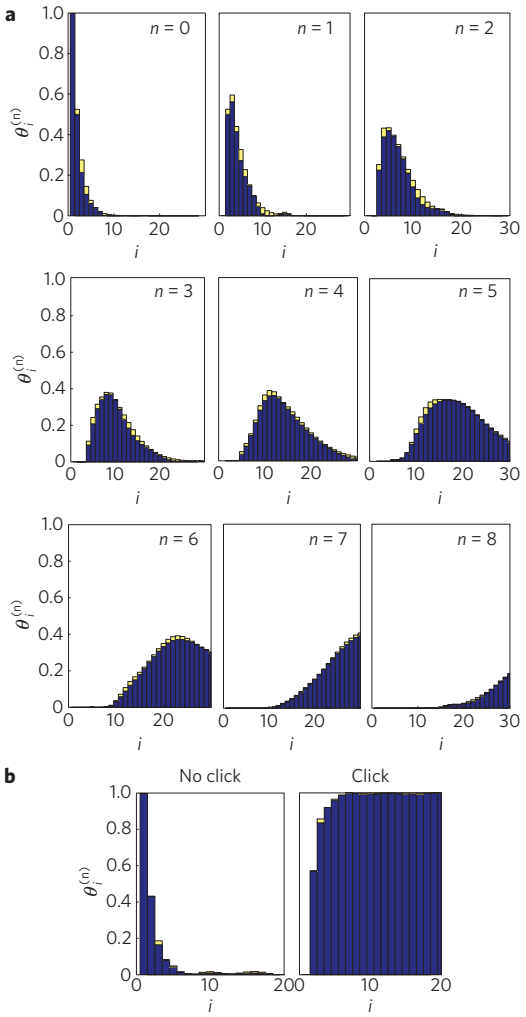

Figure 3 | Optimal physical POVMs. a,**b**, The diagonals of the reconstructed POVMs represented in the photon-number basis for the photon-number-resolving TMD (**a**) and the binary APD detector (**b**). The TMD POVM elements were obtained up to basis state $|60\rangle\langle 60|$ (therefore $M = 60$), but are shown only up to $|30\rangle\langle 30|$ for display purposes. The APD POVM elements are shown in full. Stacked on top of each $\theta_i^{(n)}$, $|\theta_i^{(n)(\mathrm{rec})} - \theta_i^{(n)(\mathrm{teo})}|$ is shown in yellow, where n is the number of clicks, and rec and teo are the reconstructed and theoretical diagonals of POVM element, π_n. The theoretical TMD and APD models are described in the Methods section.

As quantum technologies advance, detectors are becoming more complex, making a black-box approach to their characterization an important tool. Identifying the exact operations of detectors will benefit precision tasks, such as state tomography or metrology. By eliminating assumptions, full characterization enables more flexible design and use of detectors, be they noisy, nonlinear, inefficient or operating outside their normal range. With precise characterization, we can ask precise quantitative questions about our power to prepare non-classical states or herald quantum operations[21]. This opens a path for the experimental study of yet unexplored concepts such as the non-classicality of detectors. For optical detector tomography, a promising avenue for research will be to transfer well-established techniques from homodyne tomography (for example, balanced noise-reduction, direct measurement of the Wigner function or pattern functions). Now that it is well characterized, the photon counter also provides a unique tool for carrying out non-Gaussian operations,

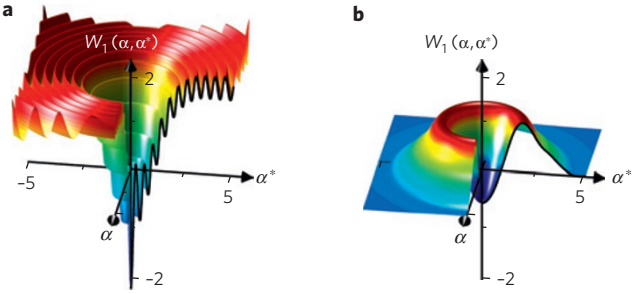

Figure 4 | The Wigner functions of the 'one click' detector outcomes. **a**,**b**, From the diagonal elements of π_1 for the APD (**a**) and TMD (**b**) one can generate the Wigner function representing their measurement of the optical mode.

which are critical for quantum information processing using the electromagnetic field as the information carrier[27,28]. As superconducting and semiconductor photon number counters are developed, tomography could be used as an objective benchmark to compare competing devices. Moreover, for one of these photon number counters, only an incomplete and empirical model is available[29], making detector tomography the best option to completely determine its action. We expect detector tomography will become the standard for the adequate calibration of all measurement and state preparation devices.

Methods

Experimental set-up. Pulses of a mode-locked laser travel through a half-wave plate ($\lambda/2$) and a Glan–Thompson polarizer with which we varied their amplitude α. We subsequently sent the pulses through a beam splitter ($T = 95\%$). The reflected beam travelled through three neutral-density (that is, spectrally flat) filters before being coupled into a single-mode fibre. The attenuation from all elements, the reflection off the beam splitter, each of the filters, and fibre coupling, were measured individually with a calibrated power meter, resulting in a total attenuation γ. This power meter was then placed in the transmission port of the beam splitter so that the magnitude of α for the probe state in the fibre was found from P, the measured time-averaged power and the pulse rate R via $|\alpha|^2 = \gamma P\lambda/(2\pi R\hbar c)$. For each value of α, we recorded the number of times each detection outcome occurred in J trials (that is, laser pulses), which provides an estimate of $p_{n,\alpha}$.

Source of light and technical noise. The input states were generated by a mode-locked Ti:sapphire laser with centre wavelength λ and a full-width at half-maximum bandwidth of $\Delta\lambda$ specifically chosen for each detector. It was cavity dumped to reduce its repetition rate R to be compatible with tested detectors. Long-term drift of the intensity over 1 million pulses was <0.5%. To characterize it, a NIST-calibrated Coherent FieldMaxII-TO power meter was used (systematic error of 5%). In the case of the APD detector (a Perkin Elmer SPCM-AQR-13-FC), we set $\lambda = 780 \pm 1$ nm, $\Delta\lambda = 20$ nm, and chose the appropriate rate $R = 1.4975 \pm 0.0005$ kHz, $J = 1472967$ and $\gamma = (5.66 \pm 0.08) \times 10^{-9}$. For the TMD detector, we set $\lambda = 789 \pm 1$ nm, $\Delta\lambda = 26$ nm, $R = 76.169 \pm 0.001$ kHz, $J = 38{,}084$ and $\gamma = (8.51 \pm 0.11) \times 10^{-9}$. We now evaluate the importance to our tomography of the technical noise found at some level in all lasers. Our laser randomly varies in energy between subsequent pulses with a standard deviation of $1.88\% \pm 0.02\%$ of $|\alpha|^2$. Attenuated to the single-photon level, as in this experiment, one might expect the inherent large fractional uncertainty in the coherent state to render this technical noise insignificant. We test this expectation by modelling the pulse distribution as a Gaussian $f_\alpha(\beta) = \mathrm{e}^{-(\beta-\alpha)^2/(2\sigma^2)}/(\sigma\sqrt{2\pi})$ centred around α in phase space, with a variance approximately equal to that measured, $\sigma^2 = 0.0004|\alpha|^4$. Each probe state is then best described by a mixture of coherent states,

$$\rho_{\langle\alpha\rangle} = \int \mathrm{d}^2\beta |\beta\rangle\langle\beta| f_\alpha(\beta) = \sum_{l,m=0}^{\infty} E_{l,m,\alpha} |l\rangle\langle m|,$$

where

$$E_{j,m,\alpha} = \frac{1}{\sigma\sqrt{2\pi}\sqrt{l!m!}} \int \beta^{l+m} \mathrm{e}^{-\beta^2-(\beta-\alpha)^2/(2\sigma^2)}\, \mathrm{d}\beta.$$

The detection probability for outcome n is then

$$p_{\langle\alpha\rangle,n} = \sum_{k=0}^{\infty} E_{k,k,\alpha}\theta_k^{(n)}.$$

Comparing our analysis done with pure input states $|\alpha\rangle\langle\alpha|$ to that done with mixed states $\rho_{\langle\alpha\rangle}$, we find the difference between the POVMs obtained was negligible. For example

$$\frac{||\Pi_{\text{pure}} - \Pi_{\text{mixed}}||_2}{||\Pi_{\text{mixed}}||_2} \leq 0.7\%$$

and the largest relative difference between any two $\theta_k^{(n)}$ coming from a mixed-state or a pure-state derivation was 1.3%. Furthermore, the reconstructed probability distributions are so close that they are indistinguishable on the scale of Fig. 1. This reinforces our earlier expectation that technical noise in the laser will be negligible when using single-photon-level coherent states. This differs from homodyne tomography where technical noise can shift a strong local oscillator to a nearly orthogonal state.

Discussion of regularization. Care has to be taken that the optimization problem is well conditioned to find the true POVM of the detector. In finding the number basis representation, we are deconvolving a coherent state from our statistics, which is intrinsically an ill-conditioned problem. Similar issues of conditioning have been discussed in the context of state and process tomography, see, for example, refs 30,31. Owing to a large ratio between the largest and smallest singular values of the matrices defining the quadratic problem, small fluctuations in the probability distribution can result in large variations for the reconstructed POVM. This can result in operators that closely approximate the outcome statistics and yet contain errant spikes in their distribution in photon number. To suppress this effect, we penalize the difference $\theta_k^{(n)} - \theta_{k+1}^{(n)}$ (independent of the shape of the POVM) by using the regularization $g = y\mathcal{S}$ with $\mathcal{S} = \sum_{k,n}[\theta_k^{(n)} - \theta_{k+1}^{(n)}]^2$. This is motivated by the fact that any realistic detector will have a finite efficiency η, which necessitates a smooth $\theta_k^{(n)}$ distribution: if $G(r)$ is the probability of registering r photons and $H(q)$ is the probability that q were present then, $G(r) = \sum_q \binom{q}{r}\eta^r(1-\eta)^{q-r}H(q)$. Consequently, if $\theta_k \neq 0$ then θ_{k+1}, θ_{k+2} and so on cannot be zero, but will follow some smooth distribution. As we do not assume any knowledge about the precise loss of our detector, we simply choose an arbitrary value for y. Varying y by three orders of magnitude hardly affects the exact value of the estimated POVM, changing it by only 10%. Furthermore, the regularization $g = y\mathcal{S}$ also proves to be robust to noise up to $\delta = 0.2$ (varying $\alpha \to \alpha(1+\delta)$ across $\{|\alpha\rangle\langle\alpha|\}$ with a Gaussian distribution for δ). This shows that the regularization's main effect is to suppress the ill-conditioning and noise while leaving the POVM fitting unaffected.

The theoretical model of the detector. Detector tomography does not make use of any physical model on the functioning of the detector. To verify the success of this approach, we have compared the outcome of the estimation to those POVM elements obtained from a theoretical model of the APD and TMD (ref. 26). The APD is treated as a binary detector with a loss of 43.2%. The theoretical TMD assumes no dark counts, three sequential beam splitters with experimentally inferred reflectivities, 50.18%, 50.60% and 41.92%, and an overall loss of 52.2% (that best fits the data), followed by two perfect APDs.

Received 16 June 2008; accepted 8 October 2008; published online 16 November 2008

References

1. Braginsky, V. R. & Khalili, F. Ya. *Quantum Measurement* 38 (Cambridge Univ. Press, 1992).
2. Luis, A. & Sanchez-Soto, L. L. Complete characterization of arbitrary quantum measurement processes. *Phys. Rev. Lett.* **83**, 3573–3576 (1999).
3. Fiurasek, J. Maximum-likelihood estimation of quantum measurement. *Phys. Rev. A* **64**, 024102 (2001).
4. D'Ariano, G. M., Maccone, L. & Lo Presti, P. Quantum calibration of measurement instrumentation. *Phys. Rev. Lett.* **93**, 250407 (2004).
5. Vogel, K. & Risken, H. Determination of quasiprobability distributions in terms of probability distributions for the rotated quadrature phase. *Phys. Rev. A* **40**, 2847–2849 (1989).
6. Smithey, D. T., Beck, M., Raymer, M. G. & Faridani, A. Measurement of the Wigner distribution and the density matrix of a light mode using optical homodyne tomography: Application to squeezed states and the vacuum. *Phys. Rev. Lett.* **70**, 1244–1247 (1993).
7. Banaszek, K., Radzewicz, C., Wodkiewicz, K. & Krasinski, J. S. Direct measurement of the Wigner function by photon counting. *Phys. Rev. A* **60**, 674–677 (1999).
8. Banaszek, K., D'Ariano, G. M., Paris, M. G. A. & Sacchi, M. F. Maximum-likelihood estimation of the density matrix. *Phys. Rev. A* **61**, 010304(R) (2000).
9. White, A. G., James, D. F. V., Munro, W. J. & Kwiat, P. G. Exploring Hilbert space: Accurate characterization of quantum information. *Phys. Rev. A* **65**, 012301 (2002).
10. Ourjoumtsev, A., Jeong, H., Tualle-Brouri, R. & Grangier, P. Generation of optical 'Schrödinger cats' from photon number states. *Nature* **448**, 784–786 (2007).
11. Neergaard-Nielsen, J. S., Melholt Nielsen, B., Hettich, C., Mølmer, K. & Polzik, E. S. Generation of a superposition of odd photon number states for quantum information networks. *Phys. Rev. Lett.* **97**, 083604 (2006).
12. Chuang, I. L. & Nielsen, M. A. Prescription for experimental determination of the dynamics of a quantum black box. *J. Mod. Opt.* **44**, 2455–2467 (1997).
13. Poyatos, J. F., Cirac, J. I. & Zoller, P. Complete characterization of a quantum process: The two-bit quantum gate. *Phys. Rev. Lett.* **78**, 390–393 (1997).
14. Altepeter, J. B. *et al.* Ancilla-assisted quantum process tomography. *Phys. Rev. Lett.* **90**, 193601 (2003).
15. D'Ariano, G. M. & Maccone, L. Measuring quantum optical Hamiltonians. *Phys. Rev. Lett.* **80**, 5465–5468 (1998).
16. Nielsen, M. A., Knill, E. & Laflamme, R. Complete quantum teleportation using nuclear magnetic resonance. *Nature* **396**, 52–55 (1998).
17. Mitchell, M. W., Ellenor, C. W., Schneider, S. & Steinberg, A. M. Diagnosis, prescription and prognosis of a Bell-state filter by quantum process tomography. *Phys. Rev. Lett.* **91**, 120402 (2003).
18. Achilles, D., Silberhorn, Ch., Sliwa, C., Banaszek, K. & Walmsley, I. A. Fiber-assisted detection with photon number resolution. *Opt. Lett.* **28**, 2387–2389 (2003).
19. Resch, K. J. *et al.* Time-reversal and super-resolving phase measurements. *Phys. Rev. Lett.* **98**, 223601 (2007).
20. Higgins, B. L., Berry, D. W., Bartlett, S. D., Wiseman, H. M. & Pryde, G. J. Entanglement-free Heisenberg-limited phase estimation. *Nature* **450**, 393–396 (2007).
21. Knill, E., Laflamme, R. & Milburn, G. J. A scheme for efficient quantum computation with linear optics. *Nature* **409**, 46–52 (2001).
22. Dunn, T., Walmsley, I. A. & Mukamel, S. Experimental determination of the quantum-mechanical state of a molecular vibrational mode using fluorescence tomography. *Phys. Rev. Lett.* **74**, 884–887 (1995).
23. O'Brien, J. L. *et al.* Quantum process tomography of a controlled-NOT gate. *Phys. Rev. Lett.* **90**, 193601 (2004).
24. Lvovsky, A. I. *et al.* Quantum state reconstruction of the single-photon Fock state. *Phys. Rev. Lett.* **87**, 050402 (2001).
25. Boyd, S. & Vandenberghe, L. *Convex Optimization* (Cambridge Univ. Press, 2004).
26. Achilles, D. *et al.* Photon-number-resolving detection using time-multiplexing. *J. Mod. Opt.* **51**, 1499–1515 (2004).
27. Eisert, J., Scheel, S. & Plenio, M. B. Distilling Gaussian states with Gaussian operations is impossible. *Phys. Rev. Lett.* **89**, 137903 (2002).
28. Browne, D. E., Eisert, J., Scheel, S. & Plenio, M. B. Driving non-Gaussian to Gaussian states with linear optics. *Phys. Rev. A* **67**, 062320 (2003).
29. Kardynal, B. E., Yuan, Z. L. & Shields, A. J. An avalanche-photodiode-based photon-number-resolving detector. *Nature Photon.* **2**, 425–428 (2008).
30. Boulant, N., Havel, T. F., Pravia, M. A. & Cory, D. G. Robust method for estimating the Lindblad operators of a dissipative quantum process from measurements of the density operator at multiple time points. *Phys. Rev. A* **67**, 042322 (2003).
31. Jezek, M., Fiurasek, J. & Hradil, Z. Quantum inference of states and processes. *Phys. Rev. A* **68**, 012305 (2003).

Acknowledgements

This work has been supported by the EU integrated project QAP and STREP COMPAS, EPSRC grants EP/C546237/1 and QIP-IRC, the Royal Society, Microsoft Research and the EURYI Award Scheme. H.C.-R. has been supported by the European Commission under the Marie Curie Programme and by the Heinz-Durr Programme of the Studienstiftung des dt. Volkes.

Author contributions

J.S.L., H.C-R. and I.A.W. contributed to the concept of the experiment and its design, as well as to laboratory measurements and data analysis. A.F., K.L.P., M.B.P. and J.E. contributed modelling and data analysis. Ch. S. and T.C.R. contributed to the conception of the project and to its planning.

Additional information

Reprints and permissions information is available online at http://npg.nature.com/reprintsandpermissions. Correspondence and requests for materials should be addressed to J.S.L. or I.A.W.